

## Thermal Cone Penetration Test (T-CPT)

Vardon, Phil; Baltoukas, Dimitris; Peuchen, Joek

**Publication date**

2018

**Document Version**

Final published version

**Published in**

Cone Penetration Testing 2018

**Citation (APA)**

Vardon, P., Baltoukas, D., & Peuchen, J. (2018). Thermal Cone Penetration Test (T-CPT). In M. A. Hicks, F. Pisano, & J. Peuchen (Eds.), *Cone Penetration Testing 2018: Proceedings of the 4th International Symposium on Cone Penetration Testing (CPT'18), 21-22 June, 2018, Delft, The Netherlands* (pp. 649-655). CRC Press.

**Important note**

To cite this publication, please use the final published version (if applicable).  
Please check the document version above.

**Copyright**

Other than for strictly personal use, it is not permitted to download, forward or distribute the text or part of it, without the consent of the author(s) and/or copyright holder(s), unless the work is under an open content license such as Creative Commons.

**Takedown policy**

Please contact us and provide details if you believe this document breaches copyrights.  
We will remove access to the work immediately and investigate your claim.

PROCEEDINGS OF THE 4<sup>TH</sup> INTERNATIONAL SYMPOSIUM ON CONE PENETRATION TESTING  
(CPT'18), DELFT, THE NETHERLANDS, 21–22 JUNE 2018

# Cone Penetration Testing 2018

*Editors*

**Michael A. Hicks**

*Section of Geo-Engineering, Department of Geoscience and Engineering,  
Faculty of Civil Engineering and Geosciences, Delft University of Technology,  
Delft, The Netherlands*

**Federico Pisanò**

*Section of Geo-Engineering, Department of Geoscience and Engineering,  
Faculty of Civil Engineering and Geosciences, Delft University of Technology,  
Delft, The Netherlands*

**Joek Peuchen**

*Fugro, The Netherlands*



**CRC Press**

Taylor & Francis Group

Boca Raton London New York Leiden

CRC Press is an imprint of the  
Taylor & Francis Group, an **informa** business

A BALKEMA BOOK

## Thermal Cone Penetration Test (T-CPT)

P.J. Vardon

*Geo-Engineering Section, Delft University of Technology, The Netherlands*

D. Baltoukas & J. Peuchen

*Fugro, The Netherlands*

**ABSTRACT:** The Thermal Cone Penetration Test (T-CPT) records temperature dissipation during an interruption of the Cone Penetration Test (CPT) to determine the thermal properties of the ground, taking advantage of heat generated in the cone penetrometer during normal operation. This paper compares two interpretation models for thermal conductivity. It is found that the thermal conductivity can be accurately determined. Care must be taken of the initial heat distribution and sensor location within the temperature cone to achieve accurate results. Furthermore, laboratory test data are presented that show that the full-displacement push of a penetrometer into sandy strata has limited influence on thermal conductivity values.

### 1 INTRODUCTION

Heat flow through the ground is of importance for applications from power cables, (shallow) geothermal energy and the storage of certain types of waste. There are currently few methods of determining the in-situ thermal properties, and those which exist either take a considerable amount of time or suffer from poor reliability or robustness.

The Thermal Cone Penetration Test (T-CPT) records temperature dissipation during an interruption of the Cone Penetration Test (CPT) to determine the thermal properties of the ground, taking advantage of heat generated in the cone penetrometer during normal operation. The T-CPT can be used over a large range of depths, unlike a needle probe, and can be taken during a CPT, thereby greatly reducing operation time. T-CPT measurements can be interpreted according to an empirically determined interpretation method (Akrouch et al., 2016) and a physics-based interpretation method (Vardon et al. 2017; the authors of this paper). This paper compares these methods.

### 2 THERMAL CONE PENETRATION TEST

The T-CPT uses a standard cone penetrometer with the addition of a temperature sensor, for example in the centre of the cone tip, as shown in Figure 1.

The T-CPT protocol is the same as for a CPT where cone tip resistance, sleeve friction and sometimes pore-pressures at various locations in the

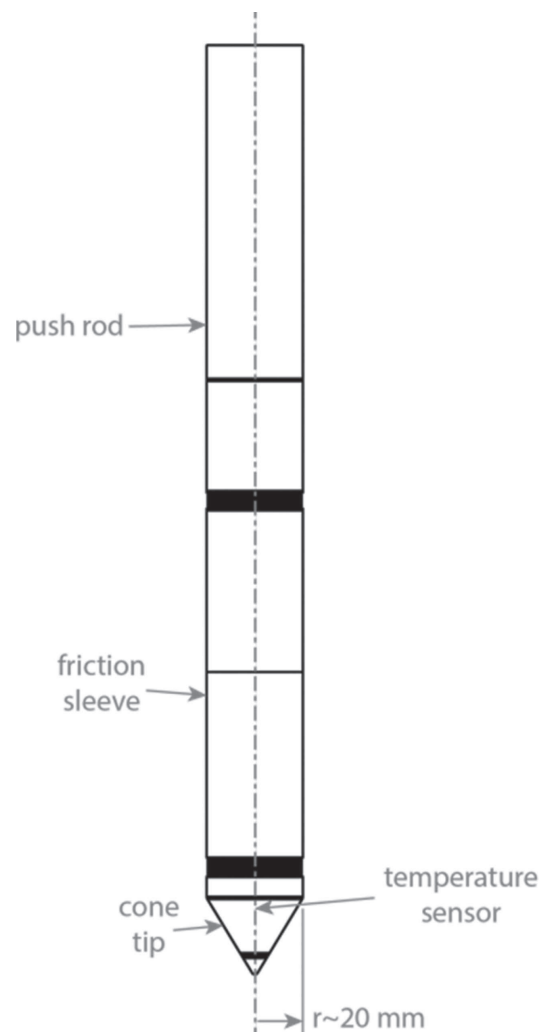


Figure 1. T-CPT cone penetrometer.

cone are measured (e.g. ISO, 2012). At the location where the thermal conductivity is required, the test is interrupted (stopped) and the temperature decay is recorded. The test is continued until the thermal conductivity converges to a good solution or until no further thermal decay is observed.

No heat source is required in the cone penetrometer and a minimum temperature difference between the ground and the cone penetrometer is required of approximately 3°C.

### 3 INTERPRETATION METHODS

#### 3.1 Physics-based interpretation method

##### 3.1.1 Principles

This method uses a 1D axisymmetric heat conduction equation. Therefore, this method should be used in situations which are dominated by conduction, as is typical in soils. Vardon et al. (2017) gave three different approximate solutions all of which gave the same final solution to determine the thermal conductivity. The simplest of these is a solution for an instantaneous heat release along a line inside a finite medium, which is given by Carslaw and Jaeger (1959) as:

$$T(r,t) = T_0 + \frac{H_0/L}{4\pi kt} \exp\left(-\frac{c_p \rho r^2}{4kt}\right) \quad (1)$$

where  $T$  is the temperature,  $r$  is the radial coordinate,  $t$  is time,  $T_0$  is the initial temperature,  $H_0/L$  is the heat release per unit length,  $k$  is the thermal conductivity,  $c_p$  is the specific heat capacity and  $\rho$  is the density.

Taking the natural logarithm and rearranging gives:

$$\ln(T - T_0) = \ln\left(\frac{H_0/L}{4\pi k}\right) - \ln(t) - \frac{c_p \rho r^2}{4kt} \quad (2)$$

and recognising that the last term is insignificant at small  $r$  and large  $t$ , leads to an expression for the thermal conductivity:

$$k = f_{TC} \frac{H_0/L}{4\pi(t(T - T_0))} \quad (3)$$

where  $f_{TC}$  is a factor included for calibration of the T-CPT cone, mainly relating to the location of the temperature sensor.

The heat content per length,  $H_0/L$ , can be calculated by:

$$H_0/L = (T_{max} - T_0)c_{p,steel}\rho_{steel}A_{cone} \quad (4)$$

where  $A_{cone}$  is the cross sectional area of the T-CPT cone and  $T_{max}$  is the maximum recorded temperature.

It can be observed that the gradient of Equation 2 with respect to  $\ln(t)$  is -1, and exploiting this leads to an expression for the initial in-situ temperature as:

$$T_0 = \frac{t_1 T_1 - t_2 T_2}{t_1 - t_2} \quad (5)$$

where the subscript 1 relates to the earlier time and 2 the later.

For all of these equations, sufficient time is required to yield a converged answer. For a typical soil this time has been seen to be between 500 and 1000 seconds. For very early times in the test the assumption of an infinite line does not hold.

Alternatively a graphical method can be used, based on Equation 2. Again recognising that at long times the last term is insignificant and that the gradient of  $\ln(T - T_0) - \ln(t)$  is -1 allows the intercept of a linear extrapolation of a  $\ln(T - T_0) - \ln(t)$  from the linear portion to the y-axis to be used in the following:

$$k = f_{TC} \frac{S(T_{max} - T_0)}{4\pi \exp(i_T)} \quad (6)$$

where  $i_T$  is the intercept. An example is shown in Figure 2, where the recorded data is shown as a curved line and the linear extrapolation is shown by the straight line.

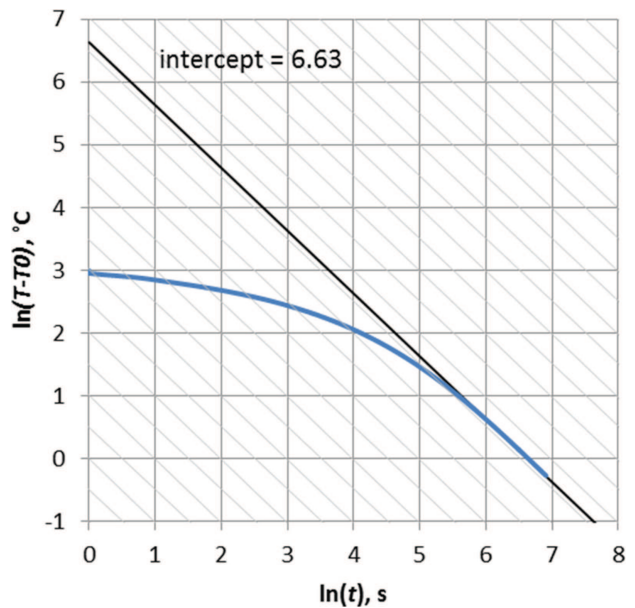


Figure 2. Example graphical method (Vardon et al. 2017).

### 3.1.2 Calibration factor

A numerical modelling study was carried out to determine the  $f_{TC}$  calibration factor. The factor corrects for two aspects: (i) the cavities in the cone penetrometer; and (ii) the location of the sensor. 1D modelling was carried out to test the working of the method, eliminating the above two effects (see Vardon et al., 2017 for details).

The model was simulated using COMSOL v5.2 using heat conduction. The geometry was 2D axisymmetric and includes a realistic geometry moderately simplified to reduce the complexity of the mesh and interior air-filled voids of the cone were removed. The mesh is presented in Figure 3.

The simulations were run in two stages, (i) a heat generation phase to represent pushing the cone through soil, and (ii) a heat dissipation stage to simulate the T-CPT. In the first stage, only the cone penetrometer was modelled (not the soil), with a heat flux boundary on the cone tip ( $500 \text{ W/m}^2$ ). In the second stage, the soil is included in the simulation and the model had a fixed temperature boundary condition of  $T_0$  at the far field and zero flux conditions at all other boundaries. Both stages simulated 1000 seconds. The initial temperature for all materials was  $20^\circ\text{C}$ . A range of thermal conductivities of the soil were simulated. The other material properties of the soil were: specific heat capacity,  $c_p = 800 \text{ J/kgK}$  and density,  $\rho = 2000 \text{ kg/m}^3$ . For the steel of the cone penetrometer they were: specific heat capacity  $c_p = 475 \text{ J/kgK}$ , density,  $\rho = 7850 \text{ kg/m}^3$  and the thermal conductivity,  $k = 44.5 \text{ W/mK}$ .

The results of a typical simulation are shown in Figure 4. The temperature dissipation after 500 seconds of the heat dissipation part of the test is shown. The temperature distribution is uneven, with higher temperatures close to the cone tip. The heat flow can be observed to be largely radial, albeit with some strong 2D effects.

The calibration factor, calculated considering only the average area of steel in the cross section

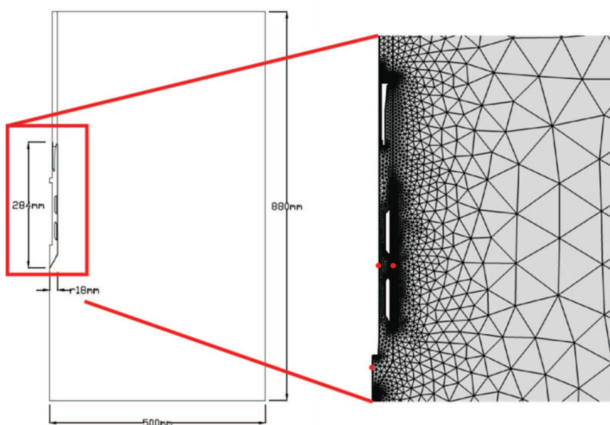


Figure 3. Domain and mesh details (Vardon et al., 2017).

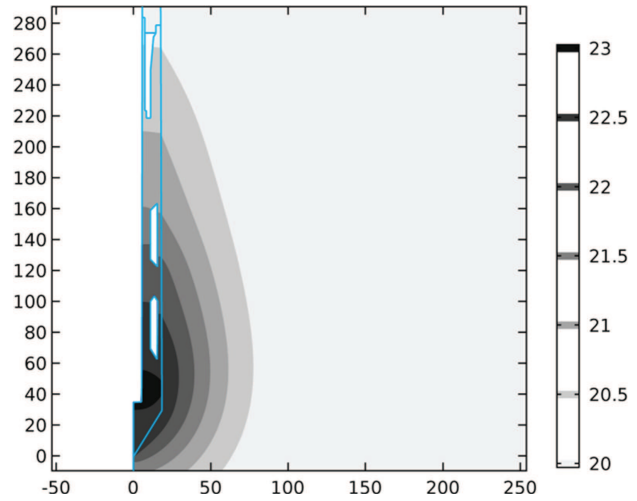


Figure 4. Contour plot of temperature (in  $^\circ\text{C}$ ) at 500 seconds, after the dissipation part of the test has begun (Vardon et al., 2017). Axes are in mm.

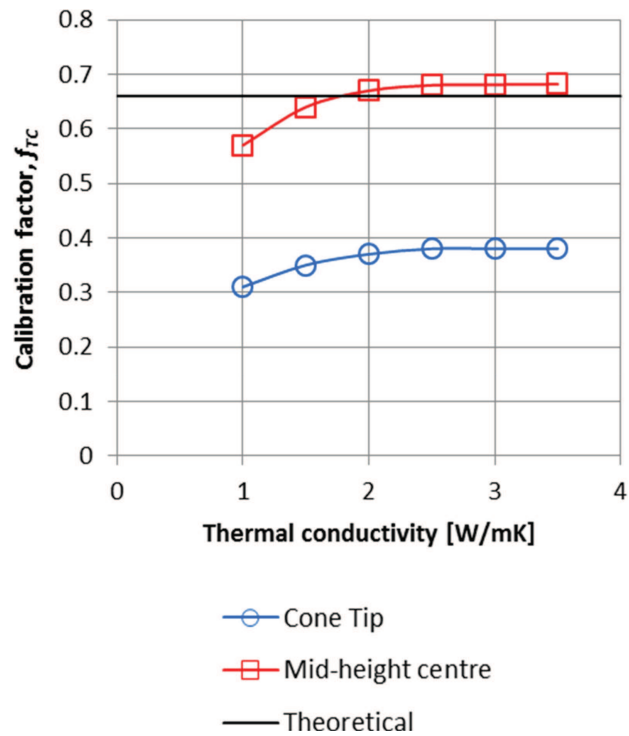


Figure 5. Calibration factor for the cone with sensor at the cone tip and mid-height (Vardon et al., 2017).

of the cone penetrometer, is 0.66. For the simulation presented here, with the temperature sensor in the cone tip, the calibration factor ranged from 0.3 to 0.38 with the thermal conductivity ranging from 1 to 3.5  $\text{W/mK}$ , as shown in Figure 5. Between thermal conductivities of 2 to 3.5  $\text{W/mK}$  the calibration factor is seen to be virtually constant. As shown, if the temperature sensor was moved to the mid-height of the cone, the calibration factor

would be close to the value correcting only for the cross sectional area.

### 3.2 Empirical interpretation method

Akrouch et al. (2016) recognised that the heat conduction and hydraulic flow equations are mathematically equivalent. They therefore proposed adopting the form of an empirical equation used to estimate the hydraulic conductivity for pore water pressure dissipation in CPTs to estimate the thermal conductivity from T-CPTs.

A numerical parametric study was carried out to calibrate the empirical equation leading to the following equation:

$$k = \frac{77}{(t_{50})^{0.968}} \quad (7)$$

where  $t_{50}$  is the time (s) for dissipation of half the initial increase in temperature and  $k$  is expressed in W/mK.

After comparing Equation 7 to experimental results the equation was modified to:

$$k = \frac{125}{t_{50}} \quad (8)$$

It is noted that both Equation 3 and 8 are inversely proportional to time, and both require knowledge of a maximum and minimum temperature. However, the empirical method requires a fictional maximum temperature, derived from a post data collection hyperbolic fit whereas the physics-based method requires simply the maximum recorded temperature.

## 4 COMPARISON OF INTERPRETATION METHODS

The two methods have been tested against the field (T-CPT) and comparative laboratory data provided by Akrouch et al. (2016) with a cone diameter of 44 mm, Data Set 1, and Vardon et al. (2017) with a cone diameter of 36 mm, Data Set 2.

### 4.1 Data set 1

Figure 6 compares the interpretation methods for the 3 sites of Data Set 1: Fugro, NGES and LA. The data was used for the calibration of the empirical method, therefore this method was expected to perform well. It is noted that the cone is a different cone than used to calculate the calibration factor for the physics-based method (Section 3.1.2), but this factor has also been used here.

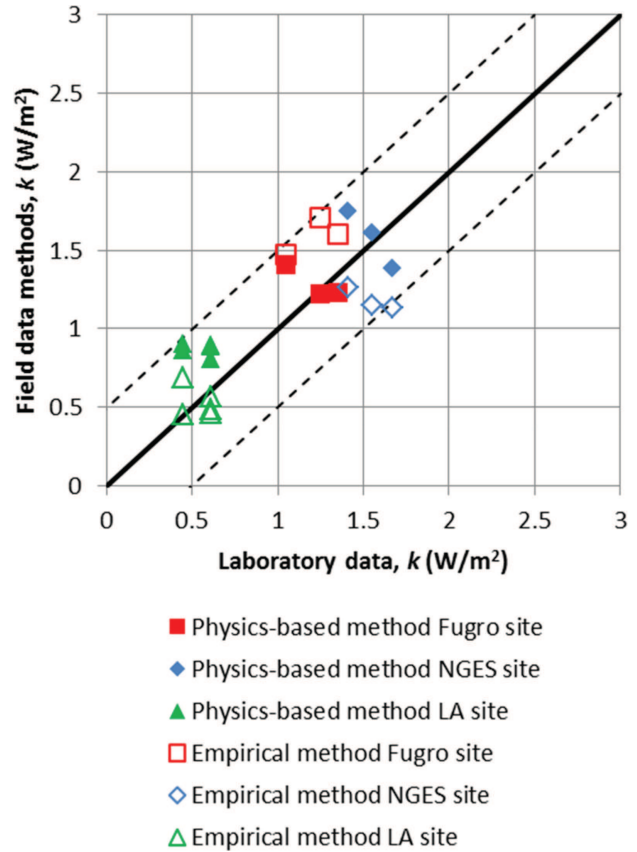


Figure 6. Comparison of interpretation methods.

It is seen that both methods can show the trends in the thermal conductivity behaviour. However, the physics-based method (shown with the solid data points) more accurately determines the difference between the Fugro and NGES sites. In general, the physics-based method slightly over-predicts the values (they are above the black line), which suggests that this cone has a marginally lower calibration factor, although it is thought likely that sampled material may have slightly desaturated.

The observed inability of the empirical method to demonstrate the difference between the Fugro and NGES sites is attributed to a higher heat capacity of the soil at the Fugro site, of about 10 to 15%. The empirical method utilises a  $t_{50}$  value (the time taken for the elevated cone temperature to dissipate to half its value) and, as illustrated in Equation 2, the heat capacity plays an important role early in the test. The heat capacity was considered in the empirical model, but only in the calculation of the constants in Equations 7 and 8, and therefore does not distinguish between soils with different heat capacities.

Further differences between the two methods are that the empirical method requires a hyperbolic curve fitting procedure to determine  $T_{max}$  and

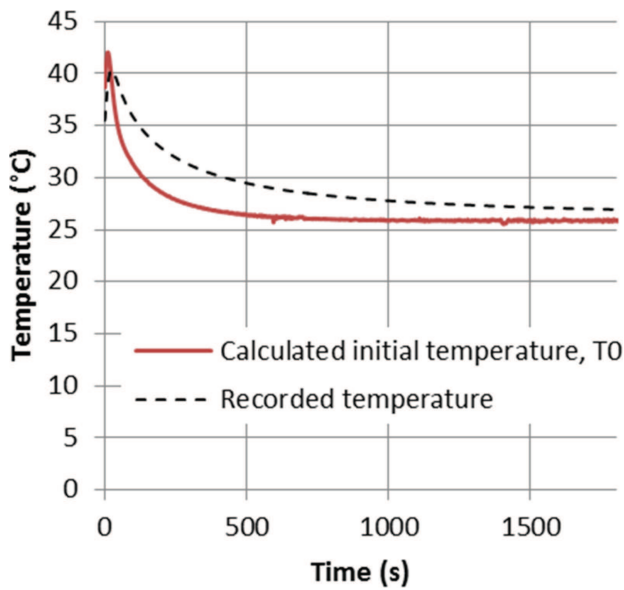


Figure 7.  $T_0$  determination for Fugro site, 8.6 m depth.

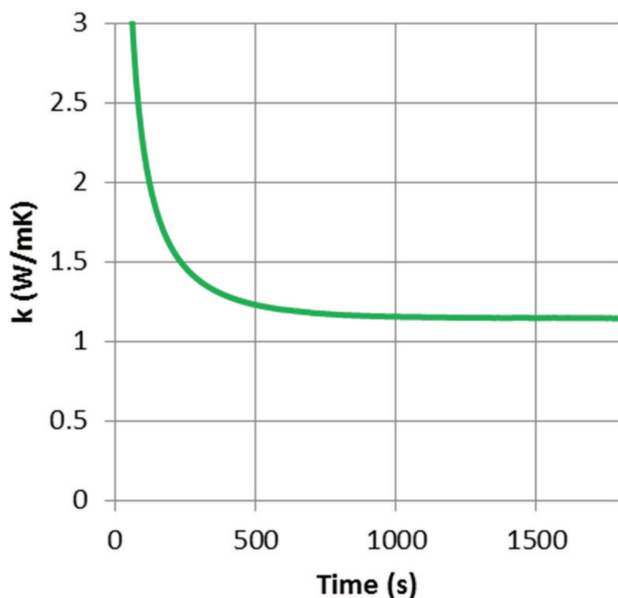


Figure 8.  $k$  determination for Fugro site, 8.6 m depth.

$T_0$ .  $T_{max}$  in this case is not the maximum recorded temperature as defined in Section 3.1.1, but a fictional maximum from the hyperbolic fit. The hyperbolic fit utilises all of the data taken in this test to gain a good fit, i.e. 1800 seconds, whereas Equation 5 is seen to determine this same value in around 600 seconds (25.90°C), as shown in Figure 7, in contrast to the recorded temperature which does not reach this in-situ temperature even at 1800 seconds.

The calculated value of thermal conductivity for the physics-based method is also seen to converge in the same time as  $T_0$  (around 600 seconds), as shown in Figure 8, indicating that the test could

be reduced in time, by up to a factor of 3 for both methods.

#### 4.2 Data Set 2

Data Set 2 covers four different methods: (i) T-CPT, (ii) in-situ thermal needle probe, (iii) thermal needle probe on sampled material, tested immediately after sampling, and (iv) thermal needle probe on sampled material in the laboratory, including undisturbed, reconstituted and multiple density tests. The T-CPTs were undertaken as CPTU according to ISO (2012), stopped at the selected test depths, and the temperatures recorded. The thermal needle probe tests were performed according to the ASTM (2014) D 5334-14 standard. The soil profiles at the test locations were mainly sand, but at some locations clay is located close to the ground surface. The calibration factor  $f_{TC} = 0.35$  was used in all cases, matching a thermal conductivity of 2 W/mK, as an a priori best estimate of thermal conductivity.

Only select results from in-situ tests are presented here for clarity and brevity. Four different locations are shown in Figures 8 to 10 with a range of depths from 5 m to 35 m. The thermal needle probe tests and the T-CPTs were generally a few metres apart horizontally at each location, and in Figure 10 the sub-locations were up to 10 m apart. It was not always possible to do tests at the same depth, as in deeper locations where the T-CPT could easily take tests the in-situ needle probe proved fragile and in shallower depths a sufficient temperature increase in the cone was not always achieved. At location 4a, to compensate for the lack of comparable results at depth, a borehole was drilled and an in-situ needle probe was taken below the bottom of the borehole at about 34 m depth.

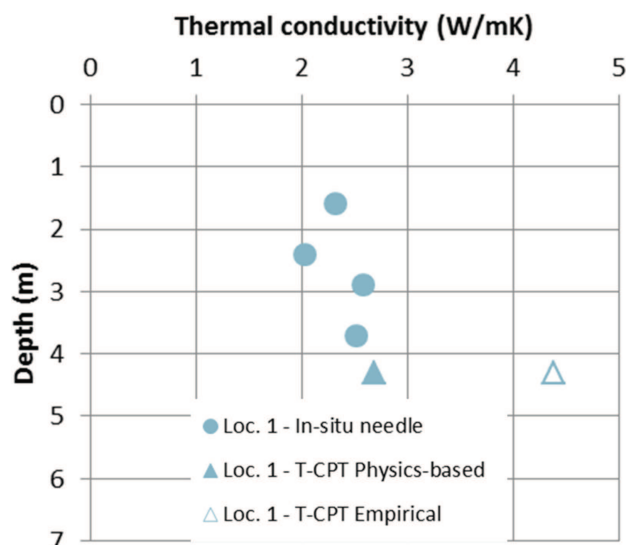


Figure 8. Thermal conductivity results at location 1.

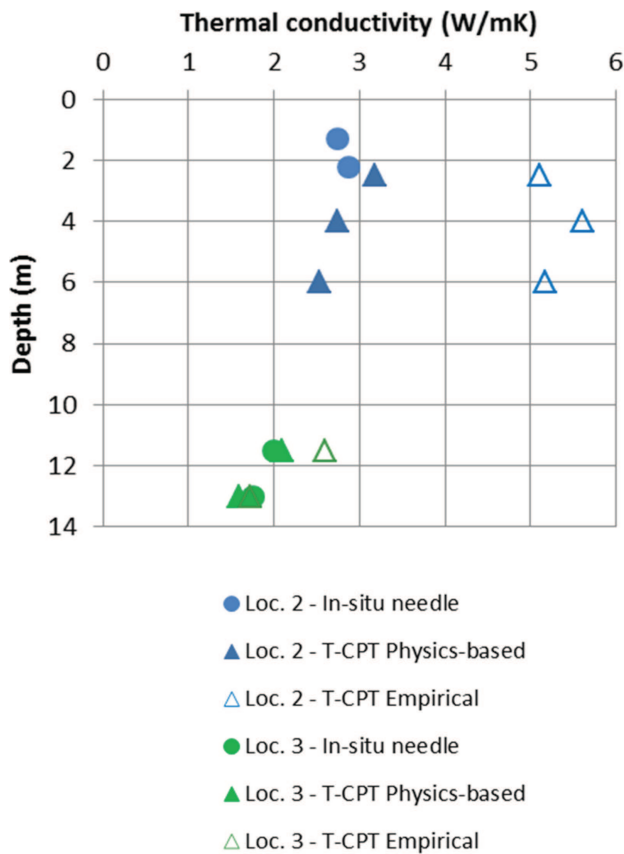


Figure 9. Thermal conductivity results at locations 2 and 3.

All figures show excellent agreement between the physics-based method and the in-situ needle probe tests, with a range of depths and thermal conductivities. The empirical method generally significantly overestimates the thermal conductivities, with the exception of location 3. However, it is observed that between tests at the same location a reasonable comparative trend is observed, see Figure 10 (location 4). It is thought that the overestimates are due to a number of factors, including the reduced cone radius (a lower initial heat content) and the wider range of thermal conductivities. In all cases the  $t_{50}$  values for Data Set 2 were significantly lower than for Data Set 1, due mainly to lower amount of heat contained in the smaller diameter cone. It is thought that while the empirical method proposed a single equation, each cone would have different parameters.

In all cases the thermal conductivity changes over the soil depth profile. This is consistent with changes in density (generally increasing, due to increasing overburden stresses), and with a variation due to soil material changes. In particular, CPTU interpretation shows clay near surface and sand at greater depths for locations 1, 2 and 4, and in location 3 a small clay layer was observed at 13 m giving a lower thermal conductivity.

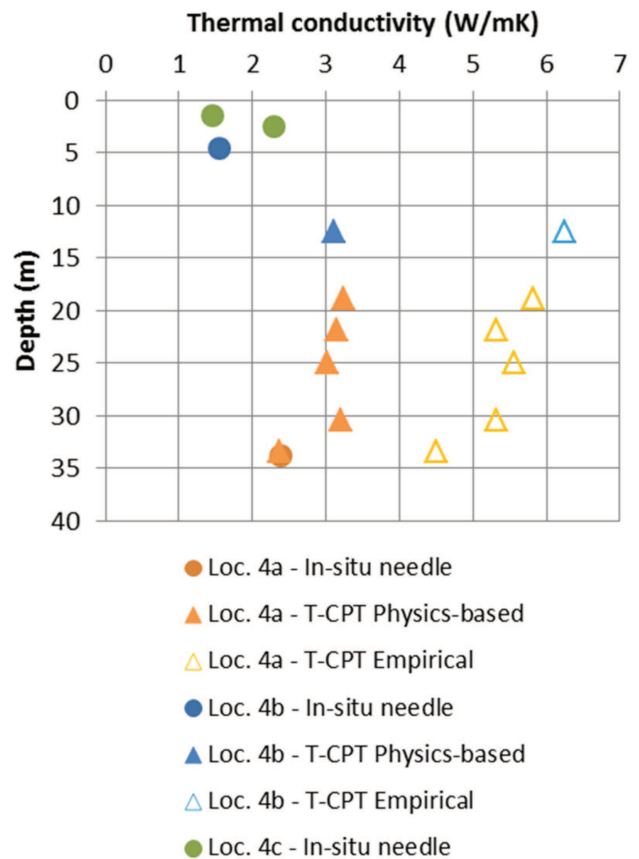


Figure 10. Thermal conductivity results at location 4.

## 5 INFLUENCE OF SAND DENSITY

In comparison to a needle probe, a cone penetrometer has a large diameter, therefore increased soil disturbance applies. The rate of penetrometer insertion is typically 20 mm/s (ISO, 2012), which, in fine grained soils, results in undrained deformations, i.e. largely without volume change. However, for sandy soils, drained conditions may apply. It is noted that heat moves through both the fluid and solid parts of soil and therefore the structure is of a lesser importance.

The zone of influence of a CPT in sandy soil depends on particle size distribution, in-situ stress conditions and drainage. It has been estimated to be up to 8 cone diameters horizontally (Mel'nikov & Boldyrev, 2015). Even in dry sand volumetric strains are small, with both contractive and expansive strains being less than 2% outside  $\sim 0.2$  cone diameters (Mel'nikov & Boldyrev, 2015).

The thermal zone of influence (Figure 5) is approximately 2 cone diameters within the part of the test needed to calculate the thermal conductivity.

Figure 11 presents example results of laboratory tests undertaken to investigate the sand density aspect. The thermal conductivity tests were



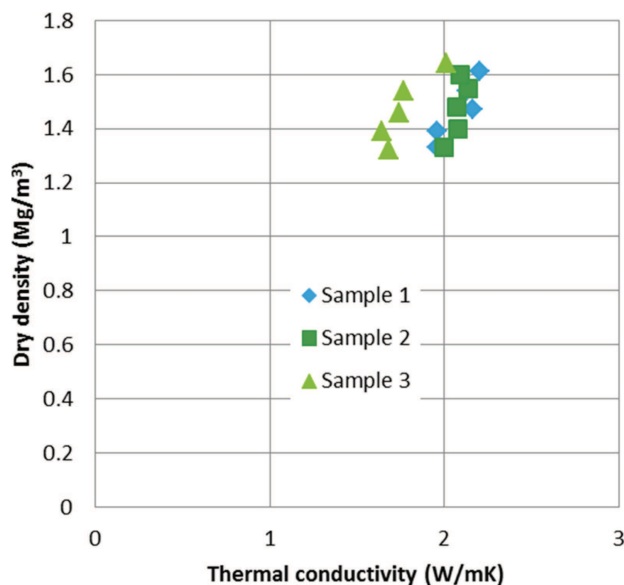


Figure 11. Thermal conductivity against density for 3 samples.

performed using a KD2 Pro Thermal Properties Analyzer (Decagon Devices, Inc.) with a TR-1 thermal needle probe (100 mm length, 2.4 mm diameter), according to ASTM (2014). The samples had dry densities from  $\sim 1.3$  to  $\sim 1.6$  Mg/m<sup>3</sup>, so representing about a  $\pm 10\%$  volumetric strain from the mean. The initially moist samples were flooded with water and subjected to increasing densification by means of a vibrating table. The thermal conductivities for each sample have an average range of 0.24 W/mK and therefore for a 2% volumetric strain the approximate difference would be approximately 0.02 W/mK, which is within the measurement error.

While using a cone penetrometer to take in-situ measurements may have a limited error due to density changes, this is thought to be significantly less than that of taking samples, which were found, in general, to exhibit slightly lower thermal conductivity values than the field tests, attributed mainly to total stress relief upon sampling and de-saturation.

## 6 CONCLUSIONS

This paper compares two interpretation methods for deriving in-situ thermal conductivity of soil from a cone penetrometer equipped with a temperature sensor. The test method (T-CPT) relies on a temperature rise in the steel of the penetrometer during a cone penetration test and subsequent measurement of temperature decay during a pause in penetration. The test equipment is more robust than needle probe type tests and therefore allows thermal conductivity to be measured at depth, without tools being swapped. The physics-based method is shown to reliably measure the thermal conductivity over a wide range of conditions and requires only spreadsheet-type analysis to be undertaken. A method of predicting the initial in-situ temperature is also shown allowing the test to be undertaken in a significantly reduced time.

## REFERENCES

- Akrouh, G.A., Briaud, J.-L., Sanchez, M. & Yilmaz, R. 2016. Thermal cone test to determine soil thermal properties, *Journal of Geotechnical and Geoenvironmental Engineering*, 142(3): 04015085.
- ASTM 2014. D 5334-14 *Standard test method for determination of thermal conductivity of soil and soft rock by thermal needle probe procedure*. ASTM.
- Carslaw, H.S. & Jaeger, J.C. 1959. *Conduction of heat in solids*, 2nd Edition, Oxford University Press, pp. 509.
- ISO 2012. *EN ISO 22476-1:2012 Geotechnical investigation and testing. Field testing. Electrical cone and piezocone penetration test*. ISO.
- Mel'nikov, A.V. & Boldyrev, G.G. 2015. Deformation Pattern of Sand Subject to Static Penetration, *Soil Mechanics and Foundation Engineering*, 51(6): 292–298.
- Vardon, P.J., Baltoukas, D. & Peuchen, J. 2017. Interpreting and validating the Thermal Cone Penetration Test (T-CPT). *Submitted to Géotechnique*.